Determining g_A/g_V with High-Resolution Spectral Measurements Using a $LiInSe_2$ Bolometer

A. F. Leder,[1,2,*] D. Mayer,[1,†] J. L. Ouellet,[1] F. A. Danevich,[3] L. Dumoulin,[4] A. Giuliani,[4] J. Kostensalo,[5] J. Kotila,[6,7,8] P. de Marcillac,[4] C. Nones,[9] V. Novati,[4] E. Olivieri,[4] D. Poda,[4] J. Suhonen,[6] V. I. Tretyak,[3] L. Winslow,[1,‡] and A. Zolotarova[9]

[1]*Massachusetts Institute of Technology, 77 Massachusetts Avenue Cambridge, Massachusetts 02139, USA*
[2]*Department of Nuclear Engineering, University of California, Berkeley, 2521 Hearst Avenue, Berkeley, California 94709, USA*
[3]*Institute for Nuclear Research of NASU, Kyiv 03028, Ukraine*
[4]*Université Paris-Saclay, CNRS/IN2P3, IJCLab, 91405 Orsay, France*
[5]*Natural Resources Institute Finland, Yliopistokatu 6B, FI-80100 Joensuu, Finland*
[6]*Department of Physics, University of Jyväskylä, P.O. Box 35, FI-40014 Jyväskylä, Finland*
[7]*Finnish Institute for Educational Research, University of Jyväskylä, P.O. Box 35, FI-40014 Jyväskylä, Finland*
[8]*Center for Theoretical Physics, Sloane Physics Laboratory Yale University, New Haven, Connecticut 06520-8120, USA*
[9]*Commissariat á l'Énergie Atomique (CEA)—Saclay, 91191 Gif-sur-Yvette, France*

(Received 18 June 2022; revised 9 August 2022; accepted 17 October 2022; published 2 December 2022)

Neutrinoless double beta decay ($0\nu\beta\beta$) processes sample a wide range of intermediate forbidden nuclear transitions, which may be impacted by quenching of the axial vector coupling constant (g_A/g_V), the uncertainty of which plays a pivotal role in determining the sensitivity reach of $0\nu\beta\beta$ experiments. In this Letter, we present measurements performed on a high-resolution $LiInSe_2$ bolometer in a "source = detector" configuration to measure the spectral shape of the fourfold forbidden β decay of ^{115}In. The value of g_A/g_V is determined by comparing the spectral shape of theoretical predictions to the experimental β spectrum taking into account various simulated background components as well as a variety of detector effects. We find evidence of quenching of g_A/g_V at $> 5\sigma$ with a model-dependent quenching factor of 0.655 ± 0.002 as compared to the free-nucleon value for the interacting shell model. We also measured the ^{115}In half-life to be $[5.18 \pm 0.06(\text{stat})^{+0.005}_{-0.015}(\text{sys})] \times 10^{14}$ yr within the interacting shell model framework. This Letter demonstrates the power of the bolometeric technique to perform precision nuclear physics single-β decay measurements, which along with improved nuclear modeling can help reduce the uncertainties in the calculation of several decay nuclear matrix elements including those used in $0\nu\beta\beta$ sensitivity calculations.

DOI: 10.1103/PhysRevLett.129.232502

Introduction.—From the first observation of single β decay [1] through C. S. Wu's ground-breaking work to determine the vector and axial vector form of the weak interaction [2], the study of β decay has been used to elucidate the hidden world of nuclear and particle physics. Modern efforts continue this legacy, using nuclear β decay to investigate the properties of neutrino mass including its absolute scale through endpoint measurements [3–5], and possible Majorana origin through searches for $0\nu\beta\beta$ [6–14].

In recent years, cryogenic bolometers have established themselves as a powerful technology in rare event searches for $0\nu\beta\beta$ [7,9–14], direct dark matter detection [15–17], and more [18–22]. Bolometers benefit from excellent energy resolution, high electron containment efficiencies, low energy trigger thresholds, and strong particle identification capabilities when equipped with a dual heat and light or heat and ionization readout [13,21,23]. Additionally, the wide variety of crystalline materials that can be practically grown allows for the study of a multitude of rare-event processes.

Theoretical calculations of the nuclear physics contributions to the $0\nu\beta\beta$ half-life have often assumed [24] an axial-to-vector coupling ratio equal to that of the free neutron, $g_A/g_V = 1.276$ [25,26], though quenched values are used to obtain agreement with observed single-β transition rates [27–30]. The exact impact on $0\nu\beta\beta$ will depend on the underlying physics of axial quenching [31]; for example, [32] provided evidence that the inclusion of two-nucleon currents and additional correlations within light nuclei ($A \leq 14$) may explain certain super-allowed heavy nuclei β-decay transitions. Axial quenching creates a significant potential systematic uncertainty in the interpretation of any $0\nu\beta\beta$ search when converting isotope-specific half-lives back to the underlying physics of interest [33], in addition to the existing uncertainties for calculated nuclear matrix elements (NMEs) for $0\nu\beta\beta$ isotopes [34].

As discussed in [35], the *shape* of highly forbidden β-decay spectra can be very sensitive to g_A/g_V, and decays of nuclei with $A \sim 100$ could shed light on g_A/g_V quenching in a similar nuclear environment as that found in $0\nu\beta\beta$ decays. This analysis technique could also have applications in explaining reactor flux anomalies through examination of first-order forbidden β-decay transitions [36]. This technique was first used to measure the decay spectrum of ^{113}Cd in [37], later experimental data from a $CdWO_4$ scintillation detector [38] were compared to theoretical spectra in order to extract a value for g_A in the range of 0.90–0.93. More recently, COBRA has applied this method to analyze data of CdZnTe detectors in order to obtain a range for g_A between 0.92 and 0.96 depending on the theoretical models used [39]. Bolometers have also shown great promise to examine other highly forbidden long-lived β-decay isotopes including ^{50}V [40]. In this Letter, we make a precision β-decay spectral shape measurement of the fourfold forbidden β decay of $^{115}\mathrm{In} \rightarrow {}^{115}\mathrm{Sn}$ ($Q_\beta = 497.489$ keV [41] and $T_{\frac{1}{2}}^{^{115}\mathrm{In}} = (4.41 \pm 0.25) \times 10^{14}$ yr [42]) using a high-resolution bolometer. This decay occurs in a mass range relevant to $0\nu\beta\beta$ isotopes and provides a benchmark to test whether many-body nuclear calculations are capable of simultaneously explaining the β-decay spectral shape and rate. Recently, interest has been growing to measure this particular ^{115}In decay mode by examining an In_2O_3 bolometer in order to provide a measurement of g_A/g_V [43].

Methods.—The $LiInSe_2$ crystal was grown by RMD Inc. [44] using the vertical Bridgeman process [45,46] and contains a natural abundance of ^{115}In of 95.72% [47]. The crystal was enriched in ^{6}Li to 95% for potential use as a neutron detector [48,49], which does not affect the β-decay analysis presented here. The $LiInSe_2$ crystal was instrumented with a neutron transmutation doped (NTD) thermistor [50], and installed inside a cryostat at IJCLab (ex. CSNSM) in Orsay, France [51], see Fig. 1. The $LiInSe_2$ scintillation signal was monitored by a separate Neganov-Trofimov-Luke Ge light detector (LD) [52], which allowed us to perform particle identification and pile-up rejection. For a full listing of experimental parameters see Table I.

The data was processed using the APOLLO and DIANA software developed by the CUORE [53], CUPID-0 [54], and CUORICINO [55] Collaborations. Events are triggered with the optimum trigger (OT) [56] and processed following a procedure similar to [10,53]. The trigger threshold was determined by injecting a series of low energy pulses through the attached Joule heater [57], achieving ~100% trigger efficiency above 20 keV. The $LiInSe_2$ detector is calibrated with a set of dedicated runs with a ^{133}Ba source using the four most prominent γ peaks in the energy range 250–400 keV.

The internal ^{115}In decay results in an expected event rate of ≈1.2 Hz in the $LiInSe_2$ detector. The recovery time after an event is ~200 ms, and the event window around each event includes 100 ms before the trigger and 500 ms after. This leads to a significant paralyzable dead time and means that internal pile-up events are expected to be a significant background.

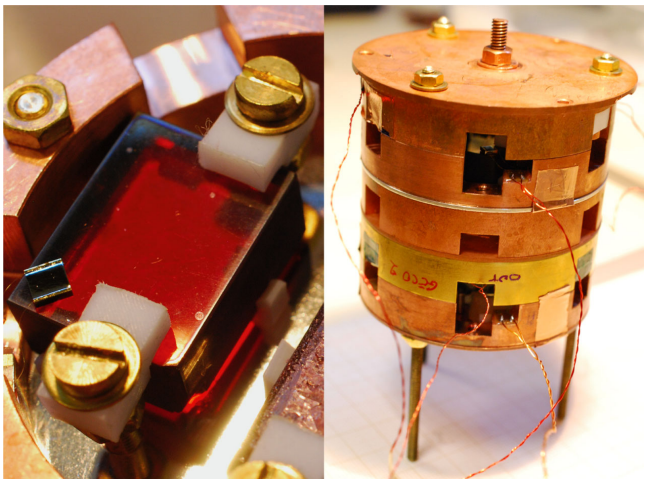

FIG. 1. Left: $LiInSe_2$ bolometer with an NTD thermistor attached to the crystal. Right: the combined detector setup in a tower configuration with two pairs of bolometers stacked in two stages. The light detector is placed above each "stage" of the tower for maximum photon absorption.

In order to filter out poorly reconstructed events from ^{115}In β^- events, a series of loose pulse shape cuts were employed. To further improve data quality, a pulse rise time cut (see Fig. 2) was defined by a 3σ band determined by fitting the rise time profiles across each energy bin. The LD also allows us to tag α events through light-yield cuts. We also employ a coincidence cut, taking advantage of the faster response time of the LD, that enforces a single-event criterion to help with filtering out pile-up events. We require that an event is only included in our spectrum if it triggers both the $LiInSe_2$ and the LD within 20 ms and no other events are recorded on the $LiInSe_2$ detector within a

TABLE I. Experimental parameters of the $LiInSe_2$ crystal during the October–November 2017 data runs.

Detector parameter	$LiInSe_2$ crystal
Crystal dimensions	$1.3 \times 1.6 \times 0.7$ cm
Total crystal mass	10.3 grams
Effective ^{115}In mass	4.1 grams
Noise level	1.1 keV (1σ)
Avg. energy resolution	2.4 keV (1σ)
100% Trigger threshold	20.0 keV
Analysis threshold	160 keV
Containment efficiency	96.6% @ 497 keV
Data selection cut efficiency	47.6(2)% (160–500 keV)
Livetime fraction	52.54(8)%
Total exposure	39.7 g days

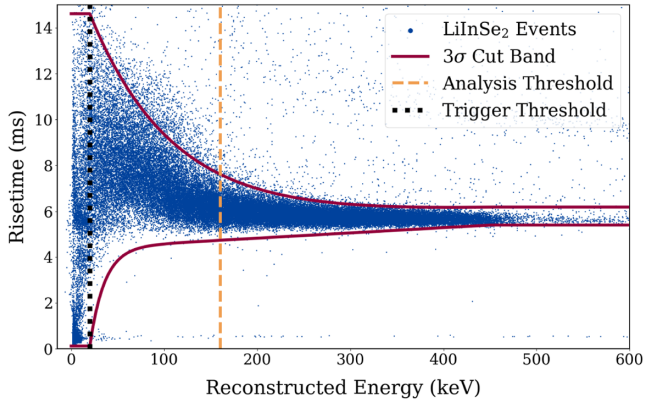

FIG. 2. LiInSe$_2$ detector events with 3σ cut bands, analysis and trigger thresholds superimposed. The corresponding rise time cut band was calculated by interpolating between the 3σ Gaussian bin profile in 10 keV energy bins running between 20–450 keV. Outside of this energy range, the cut values were kept constant due to large uncertainties in the profile fit as a result of non-Gaussian parameter distributions (low) statistics at the low (high) energy ranges, respectively.

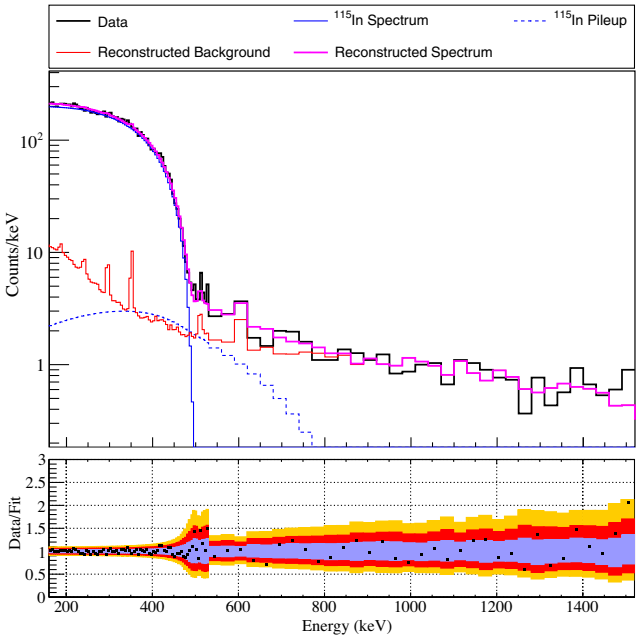

FIG. 3. Top: spectral fit to the collected LiInSe$_2$ spectrum over the region 160–1520 keV. Component normalizations and the ^{115}In spectral shape correspond to the best-fit values for the interacting shell model (ISM) exhibiting a $\chi^2 \approx 160$ with 101 degrees of freedom. Fits to the microscopic quasiparticle-phonon model (MQPM) and interacting boson model (IBM) result in similar reconstructions. Bottom: data/fit ratios for the reconstruction, along with 1σ (purple), 2σ (red), and 3σ (yellow) fit credibility regions. The spectrum is binned by 5 keV between 5–530 keV and by 30 keV above 530 keV in order to maintain reasonable statistics per bin above the ^{115}In endpoint.

broader 600 ms window. Over the region of 160–500 keV, we find a cut efficiency of $(47.6 \pm 0.2)\%$, dominated by the LD single-event criterion. The 160 keV threshold was selected as the lowest energy where multiple event pileup was well handled by the autoconvolution background component. The resulting events that pass all the above cuts are then compiled into the input LiInSe$_2$ spectrum as shown in Fig. 3.

To extract g_A/g_V from the measured LiInSe$_2$ spectrum, we follow a procedure similar to [58–61] and decompose the spectrum into various components: a model-dependent signal component from the β decay of ^{115}In dependent on g_A/g_V, an untagged pile-up component, and other radioactive background contributions. The fit is implemented using the Bayesian analysis toolkit package [62], which implements a Markov chain Monte Carlo (MCMC) to sample the full joint posterior. We perform this decomposition on the spectrum in Fig. 3, which has a binning of 5 keV below 530 and 30 keV between 530 and 1520 keV, the analysis cut-off. This binning scheme allows for the fitting of most spectral features while still maintaining the highest possible statistics per bin in the region beyond 530 keV. We also implement an analysis threshold of 160 keV to avoid low-energy pile-up events which are difficult to separate in time and can distort the spectrum.

To implement the MCMC, we define our binned likelihood as

$$\mathcal{L} = \prod_i \mathrm{Pois}\left(k_i; \sum_j a_j \lambda_{ij}\right), \tag{1}$$

enumerating bins by i and fitted components by j. Here, k_i is the number of observed counts within a given bin, λ_{ij} is the normalized density of the jth component within the ith bin, and a_j are the fitted normalizations for the different components. The densities λ corresponding to ^{115}In are g_A/g_V dependent.

Numerical calculations for the structure of ^{115}In are performed using the interacting shell model (ISM) [63–65], interacting boson model (IBM) [66], and microscopic quasiparticle-phonon model (MQPM) [67]. We generate a library of 200 discrete β-decay spectra for g_A/g_V uniformly spaced across the range $0.6 < g_A/g_V < 1.3$ and then perform an interpolation for the spectral shape for g_A/g_V values not in our library. Each ^{115}In spectrum is then convolved with an energy-dependent detector response function to account for energy losses as well as shifts in the spectral shape from β particles that escape the absorber. ThroughGEANT4 simulation [68] of the LiInSe$_2$ crystal and its neighboring copper plate we determined that 96.6% of all internally generated βs have their energies fully contained within the detector volume at the $Q_{^{115}\mathrm{In}}$ value (497 keV), which represents the minimum containment efficiency over the entire ^{115}In. Background contamination spectra are obtained via GEANT4, simulating various possible radiogenic decay chains on neighboring detector/cryostat components to our detector. In total, we simulated

the resulting γ and β spectra stemming from ^{238}U/^{232}Th decay chains from nearby cryostat components and overall environmental contamination. We also simulated internal ^{60}Co, and ^{40}K decays present uniformly throughout the $LiInSe_2$ detector. In addition, we simulated a separate background contribution coming solely from possible surface contaminations of the $LiInSe_2$ crystal. All these simulated spectra were also convolved with the $LiInSe_2$ detector's measured energy resolution before its use as a potential component of the MCMC fit. We also generated an irreducible pile-up background component (the auto-convolution of the ^{115}In β spectrum) to account for the inability to separate events which occur too closely in time and could then be misreconstructed as a single higher energy event.

The final MCMC fit only included the four most-dominant background components: (1) and (2) ^{238}U decay chains and ^{60}Co decays from internal crystal contamination, (3) ^{232}Th decay chain events on the copper plate underneath the $LiInSe_2$ crystal, and (4) ^{232}Th decay chain events (mostly γs) from external sources. α backgrounds can be safely ignored, thanks to the strong pulse shape and coincidence cuts applied to the collected data, resulting in predominantly bulk γ backgrounds. All other simulated background components were found to have only a negligible effect on the final fit parameters. This results in a satisfactory description of background features in the collected spectrum without introducing degeneracies in the fit from additional components which may not be differentiated with available data. We perform a separate fit for each nuclear model tested, and apply uniform priors to the normalizations of each fitted component within the regions of g_A/g_V discussed below.

Discussion.—For all three nuclear models examined, the likelihood function within the fit is bimodal with respect to g_A/g_V, exhibiting a local minimum both at g_A/g_V below 0.95 and again above 1.05. Fits arising from the $g_A/g_V > 1.05$ minimum result in a poor match to the observed spectral shape, with decreases in log-likelihood as compared to the $g_A/g_V < 0.95$ minimum of at least 65 (IBM), 90 (MQPM) and 118 (ISM). Despite this, the high-g_A/g_V fit minima are still sufficiently favored that without a restricted prior, the MCMC chain would still eventually achieve convergence. In order to ensure a good convergence of the MCMC chain about the global minimum while avoiding numerical instabilities, we restrict ourselves to a uniform prior on $g_A/g_V \in [0.6, 1.0]$.

We extract the best-fit values from the maximum *a posteriori* point, along with Bayesian credibility regions (BCRs) for parameters pertaining to the $T_{\frac{1}{2}}^{^{115}\mathrm{In}}$ and g_A/g_V value. We marginalize over all background component normalizations as nuisance parameters; all three fits result in compatible contributions from each of the included background components. The best-fit values for g_A/g_V along with the central 1σ BCRs arising from the fits are summarized in Table II. Unsurprisingly, the various nuclear calculations prefer different values of g_A/g_V, however, all models strongly reject the free-nucleon value of $g_A/g_V = 1.276$ at $> 5\sigma$ as determined by the $\Delta \log \mathcal{L}$ between the best-fit values and the free-nucleon value, assuming Wilk's theorem [69].

TABLE II. ^{115}In fit results for the ISM, IBM, and MQPM nuclear models. For the fitted g_A/g_V and $T_{1/2}$ values, we quote the best fit value with uncertainty given by the width of the central 68% Bayesian credibility interval, along with the reduced-χ^2 value for the best-fit reconstruction. Additional $T_{1/2}$ values for ^{115}In taken from literature are provided for reference.

Model	g_A/g_V	$T_{\frac{1}{2}}^{^{115}\mathrm{In}}$ (10^{14} yr)	Reduced χ^2
ISM	0.830 ± 0.002	5.177 ± 0.060	1.58
IBM	0.845 ± 0.006	5.031 ± 0.065	1.50
MQPM	0.936 ± 0.003	5.222 ± 0.061	1.60
Pfeiffer *et al.* [42]		4.41 ± 0.25	
Watt and Glover [70]		5.1 ± 0.4	
Beard and Kelly [71]		6.9 ± 1.5	

From our fit results, we can also extract the value of $T_{\frac{1}{2}}^{^{115}\mathrm{In}} = [5.18 \pm 0.06(\mathrm{stat})^{+0.005}_{-0.015}(\mathrm{sys})] \times 10^{14}$ yr. Here we quote the best-fit value arising from the ISM model fit, with statistical uncertainty determined by the width of the

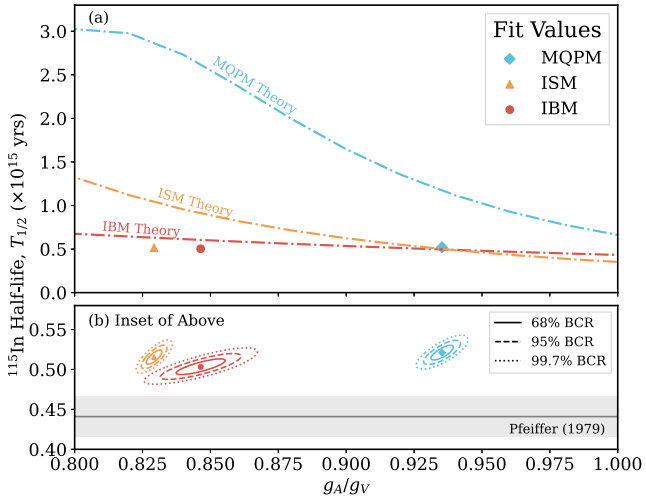

FIG. 4. (a) Half-lives versus g_A/g_V theory curves (dash-dotted lines), assuming a conserved vector current [72], for ^{115}In as well as the best fit half-lives and g_A/g_V values (markers) resulting from the spectral-shape fits for the IBM (red), ISM (yellow), and MQPM (cyan) models considered in this Letter. (b) Enlargement of (a) including previous half-life measurement from [42] in gray with 1σ uncertainty (other measurements omitted for clarity). Contours about the best fit values represent the joint two-dimensional Bayesian credibility regions produced from the fit posteriors and only include statistical uncertainties.

1σ central BCR with negligible contributions from uncertainties in the cut and live-time efficiencies. We choose to quote the spread in half-life with respect to the IBM and MQPM best-fit values (shown in Table II) as a systematic uncertainty. This is slower by 3σ with respect to [42], but falls within 2σ of the older, less precise measurements [70,71]. Figure 4(b) displays the joint two-dimensional Bayesian credibility regions for g_A/g_V and $T_{1/2}$ for each fitted nuclear model, along with the best-fit points.

We are then able to simultaneously calculate the $T_{\frac{1}{2}}$ as a function of g_A/g_V values [73] as shown by the dash-dotted lines in Fig. 4. Our best fit values for $T_{\frac{1}{2}}$ overestimate the $T_{\frac{1}{2}}$ by factors of 1.2 (IBM), 2.2 (MQPM), and 2.0 (ISM) compared to [42], and simultaneously do not fall upon their respective theory curves. This suggests that our quenching-dependent calculations are not yet able to simultaneously match the spectral shape and decay rate in ^{115}In. It is worth noting that the half-life in [42] is similarly incapable of simultaneously matching the spectral shape and decay rate.

Previous work with ^{113}Cd data has shown that this type of tension between independent measurements of half-life and quenched g_A/g_V values can be relaxed via the introduction of a small relativistic nuclear matrix element correction that affects the spectral shape due to the enforcement of the conserved vector current assumption [74]. Because of the closeness of our results with the measurements presented in [70,71], we do not present any conclusion regarding the accuracy of any single nuclear model presented here. This Letter seeks to showcase the ability of this technique to simultaneously provide two independent experimental cross-checks to any nuclear calculation framework used to model highly forbidden nuclear β decays.

Conclusion.—From these data, it is clear that the value of g_A/g_V that governs the ^{115}In highly forbidden decay is quenched by approximately 0.65–0.75 compared to the decay of the free neutron. Interestingly, for each of the nuclear models examined there is strong disagreement between the measured $T_{\frac{1}{2}}^{^{115}\mathrm{In}}$ from [42] and the predicted half-life value for the favored value of g_A/g_V calculated from spectral shape analysis. This tension could point to possible issues with regards to the many-body approaches and Hamiltonians used in the various calculation frameworks. At the same time, our better agreement with the older measurements of [70,71] may point to additional systematic effects that could be addressed in subsequent spectral shape/half-life calculations. This measurement showcases the utility of cryogenic bolometers for precision studies to test various spectral shapes calculated using different nuclear modeling frameworks for rare or forbidden nuclear processes. Further developments in fast cryogenic detectors, such as the use of transition edge sensors for heat and/or light readout, would provide better separation of low-energy pile-up events and could offer even better energy resolution than the data presented here [23,75]. Further refinements in the theory calculations of the NMEs [76,77], coupled with studies of ^{115}In and other candidate isotopes [74] (for an expanded list see [78]) could further increase the sensitivity to g_A/g_V across multiple nuclear environments. Coupled with improved nuclear modeling, this and future g_A/g_V measurements have the potential to reduce the systematic uncertainty on the NMEs for decay calculations, including those used by $0\nu\beta\beta$ experiments to determine their current and projected sensitivity limits.

The dilution refrigerator used for the tests and installed at IJCLab (Orsay, France) was donated by the Dipartimento di Scienza e Alta Tecnologia of the Insubria University (Como, Italy). This work makes use of the DIANA data analysis and APOLLO data acquisition software which has been developed by the CUORICINO, CUORE, LUCIFER, CUPID-Mo, and CUPID-0 Collaborations. A. F. L. acknowledges the support of the California Alliance Fellowship. L. W. would like to acknowledge funding from Grant No. DE-SC0011091. J. K. would like to acknowledge funding from Academy of Finland Grants No. 314733 and No. 345869. This work has also been partially supported by the Academy of Finland under the Academy Project No. 318043. F. A. D. and V. I. T. were supported in part by the National Research Foundation of Ukraine Grant No. 2020.02/0011.

*aleder@berkeley.edu
†dmayer@mit.edu
‡lwinslow@mit.edu

[1] J Chadwick, Intensitatsverteilung im magnetischen spektrum der beta-strahlen von radium B + C, Verh. Dtsch. Phys. Ges. **16**, 383 (1914).
[2] C. S. Wu, E. Ambler, R. W. Hayward, D. D. Hoppes, and R. P. Hudson, Experimental test of parity conservation in beta decay, Phys. Rev. **105**, 1413 (1957).
[3] M. Aker, K. Altenmuller, M. Arenz, M. Babutzka, J. Barret, S. Bauer *et al.*, Improved Upper Limit on the Neutrino Mass from a Direct Kinematic Method by KATRIN, Phys. Rev. Lett. **123**, 221802 (2019).
[4] M. Aker, K. Altenmuller, A. Beglarian, J. Behrens, A. Berlev, U. Besserer *et al.*, Analysis methods for the first KATRIN neutrino-mass measurement, Phys. Rev. D **104**, 012005 (2021).
[5] M. Aker, A. Beglarian, J. Behrens, A. Berlev, U. Besserer, B. Bieringer *et al.*, Direct neutrino-mass measurement with sub-electronvolt sensitivity, Nat. Phys. **18**, 160 (2022).
[6] A. Gando, Y. Gando, T. Hachiya, A. Hayashi, S. Hayashida, H. Ikeda *et al.*, Search for Majorana Neutrinos Near the Inverted Mass Hierarchy Region with KamLAND-Zen, Phys. Rev. Lett. **117**, 082503 (2016).
[7] S. I. Alvis, I. J. Arnquist, F. T. Avignone III, A. S. Barabash, C. J. Barton, V. Basu *et al.*, Search for neutrinoless double-β decay in ^{76}Ge with 26 kg yr of exposure from the Majorana

Demonstrator Search for Neutrinoless Double-β Decay, Phys. Rev. C **100**, 025501 (2019).
[8] G. Anton, I. Badhrees, P. S. Barbeau, D. Beck, V. Belov, T. Bhatta *et al.*, Search for Neutrinoless Double-β Decay with the Complete EXO-200 Dataset, Phys. Rev. Lett. **123**, 161802 (2019).
[9] M. Agostini, G. R. Araujo, A. M. Bakalyarov, M. Balata, I. Barabanov, L. Baudis *et al.*, Final Results of GERDA on the Search for Neutrinoless Double-β Decay, Phys. Rev. Lett. **125**, 252502 (2020).
[10] D. Q. Adams, C. Alduino, K. Alfonso, F. T. Avignone III, O. Azzolini, G. Bari *et al.*, Improved Limit on Neutrinoless Double-Beta Decay in ^{130}Te with CUORE, Phys. Rev. Lett. **124**, 122501 (2020).
[11] D. Q. Adams, C. Alduino, K. Alfonso, F. T. Avignone III, O. Azzolini, G. Bari *et al.*, Search for Majorana neutrinos exploiting millikelvin cryogenics with CUORE, Nature (London) **604**, 53 (2022).
[12] E. Armengaud, C. Augier, A. S. Barabash, F. Bellini, G. Benato, A. Benoit *et al.*, New Limit for Neutrinoless Double-Beta Decay of ^{100}Mo from the CUPID-Mo Experiment, Phys. Rev. Lett. **126**, 181802 (2021).
[13] O. Azzolini, J. W. Beeman, F. Bellini, M. Beretta, M. Biassoni, C. Brofferio *et al.*, Final Result of CUPID-0 Phase-I in the Search for the ^{82}Se Neutrinoless Double-β Decay, Phys. Rev. Lett. **123**, 032501 (2019).
[14] V. Alenkov, H. W. Bae, J. Beyer, R. S. Boiko, K. Boonin, O. Buzanov *et al.*, First results from the AMoRE-Pilot neutrinoless double beta decay experiment, Eur. Phys. J. C **79**, 791 (2019).
[15] A. H. Abdelhameed, G. Angloher, P. Bauer, A. Bento, E. Bertoldo, C. Bucci *et al.*, First results from the CRESST-III low-mass dark matter program, Phys. Rev. D **100**, 102002 (2019).
[16] I. Alkhatib, D. W. P Amaral, T. Aralis, T. Aramaki, I. J. Arnquist, I. Ataee Langroudy *et al.*, Light Dark Matter Search with a High-Resolution Athermal Phonon Detector Operated above Ground, Phys. Rev. Lett. **127**, 061801 (2021).
[17] R. Agnese, T. Aralis, T. Aramaki, I. J. Arnquist, E. Azadbakht, W. Baker *et al.*, Search for low-mass dark matter with CDMSlite using a profile likelihood fit, Phys. Rev. D **99**, 062001 (2019).
[18] C. Augier, G. Beaulieu, V. Belov, L. Berge, J. Billard, G. Bres *et al.*, Ricochet progress and status, arXiv:2111.06745.
[19] I. Alkhatib, D. W. P Amaral, T. Aralis, T. Aramaki, I. J. Arnquist, I. Ataee Langroudy *et al.*, Constraints on Lightly Ionizing Particles from CDMSlite, Phys. Rev. Lett. **127**, 081802 (2021).
[20] M. Pyle, E. Figueroa-Feliciano, and B. Sadoulet, Optimized designs for very low temperature massive calorimeters, arXiv:1503.01200.
[21] Denys Poda, Scintillation in low-temperature particle detectors, Physics **3**, 473 (2021).
[22] P. De Marcillac, N. Coron, G. Dambier, J. Leblanc, and J. Moalic, Experimental detection of α-particles from the radioactive decay of natural bismuth, Nature (London) **422**, 876 (2003).
[23] R. Huang, E. Armengaud, C. Augier, A. S. Barabash, F. Bellini, G. Benato *et al.*, Pulse shape discrimination in CUPID-Mo using principal component analysis, J. Instrum. **16**, P03032 (2021).
[24] J. Barea, J. Kotila, and F. Iachello, Nuclear matrix elements for double beta decay, Phys. Rev. C **87**, 014315 (2013).
[25] D. Mund, B. Märkisch, M. Deissenroth, J. Krempel, M. Schumann, H. Abele, A. Petoukhov, and T. Soldner, Determination of the Weak Axial Vector Coupling $\lambda = (g_A/g_V)$ from a Measurement of the β-Asymmetry Parameter A in Neutron Beta Decay, Phys. Rev. Lett. **110**, 172502 (2013).
[26] B. Markisch, H. Mest, H. Saul, X. Wang, H. Abele, D. Dubbers, M. Klopf, A. Petoukhov, C. Roick, T. Soldner, and D. Werder, Measurement of the Weak Axial-Vector Coupling Constant in the Decay of Free Neutrons Using a Pulsed Cold Neutron Beam, Phys. Rev. Lett. **122**, 242501 (2019).
[27] V. Kumar, P. C. Srivastava, and H. Li, Nuclear β-decay half-lives for fp and fpg shell nuclei, J. Phys. G **43**, 105104 (2016).
[28] W. T. Chou, E. K. Warburton, and B. A. Brown, Gamow-Teller beta-decay rates for A<18 nuclei, Phys. Rev. C **47**, 163 (1993).
[29] B. Brown, Status of the nuclear shell model, Annu. Rev. Nucl. Part. Sci. **38**, 29 (1988).
[30] G. Martínez-Pinedo, A. Poves, E. Caurier, and A. P. Zuker, Effective g_A in the pf shell, Phys. Rev. C **53**, R2602 (1996).
[31] J. Suhonen, Value of the axial-vector coupling strength in β and $\beta\beta$ decays: A review, Front. Phys. **5**, 55 (2017).
[32] P. Gysbers, G. Hagen, J. D. Holt, G. R. Jansen, T. D. Morris, P. Navratil, T. Papenbrock, S. Quaglioni, A. Schwenk, S. R. Stroberg, and K. A. Wendt, Discrepancy between experimental and theoretical β-decay rates resolved from first principles, Nat. Phys. **15**, 428 (2019).
[33] M. J. Dolinski, A. W. Poon, and W. Rodejohann, Neutrinoless double-beta decay: Status and prospects, Annu. Rev. Nucl. Part. Sci. **69**, 219 (2019).
[34] J. Engel and J. Menéndez, Status and future of nuclear matrix elements for neutrinoless double-beta decay: A review, Rep. Prog. Phys. **80**, 046301 (2017).
[35] M. Haaranen, P. C. Srivastava, and J. Suhonen, Forbidden nonunique beta decays and effective values of weak coupling constants, Phys. Rev. C **93**, 034308 (2016).
[36] L. Hayen, J. Kostensalo, N. Severijns, and J. Suhonen, First-forbidden transitions in the reactor anomaly, Phys. Rev. C **100**, 054323 (2019).
[37] A. Alessandrello, C. Brofferio, D. V. Camin, O. Cremonesi, F. A. Danevich, P. de Marcillac *et al.*, Bolometric measurement of the beta spectrum of ^{113}Cd, Nucl. Phys. B, Proc. Suppl. **35**, 394 (1994).
[38] P. Belli, R. Bernabei, N. Bukilic, F. Cappella, R. Cerulli, C. J. Dai *et al.*, Investigation of β decay of ^{113}Cd, Phys. Rev. C **76**, 064603 (2007).
[39] L. Bodenstein-Dresler, Y. Chu, D. Gehre, C. Gossling, A. Heimbold, C. Herrmann *et al.*, Quenching of g_A deduced from the β-spectrum shape of ^{113}Cd measured with the COBRA experiment, Phys. Lett. B **800**, 135092 (2020).
[40] L. Pattavina, M. Laubenstein, S. S. Nagorny, S. Nisi, L. Pagnanini, S. Pirro, C. Rusconi, and K. Schäffner, An

innovative technique for the investigation of the 4-fold forbidden beta-decay of ^{50}V, Eur. Phys. J. A **54**, 79 (2018).
[41] M. Wang, W. J. Huang, F. G. Kondev, G. Audi, and S. Naimi, The AME 2020 atomic mass evaluation (II). Tables, graphs and references, Chin. Phys. C **45**, 030003 (2021).
[42] L. Pfeiffer, A. P. Mills, E. A. Chandross, and T. Kovacs, Beta spectrum of ^{115}In, Phys. Rev. C **19**, 1035 (1979).
[43] E. Celi, Z. Galazka, M. Laubenstein, S. Nagorny, L. Pagnanini, S. Pirro, and A. Puiu, Development of a cryogenic In_2O_3 calorimeter to measure the spectral shape of ^{115}In β-decay, Nucl. Instrum. Methods Phys. Res., Sect. A **1033**, 166682 (2022).
[44] 44 Hunt Street, Watertown, Massachusetts 02472, email: info@rmdinc.com, website: rmdinc.com.
[45] L. Isaenko, I. Vasilyeva, A. Merkulov, A. Yelisseyev, and S. Lobanov, Growth of new nonlinear crystals $LiMX_2$(M = Al, In, Ga; X = S, Se, Te) for the mid-IR optics, J. Cryst. Growth **275**, 217 (2005).
[46] J. Tower, L. Winslow, A. Churilov, Y. Ogorodnik, H. Hong, J. Glodo *et al.*, New scintillating bolometer crystals for rare particle detection, Nucl. Instrum. Methods Phys. Res., Sect. A **954**, 162300 (2020).
[47] J. Meija, T. Coplen, M. Berglund, W. Brand, P. De Bievre, M. Gröning, N. E. Holden, J. Irrgeher, R. D. Loss, T. Walczyk, and T. Prohaska, Isotopic compositions of the elements 2013 (IUPAC Technical Report), Pure Appl. Chem. **88**, 293 (2016).
[48] Z. W. Bell, A. Burger, L. Matei, M. Groza, A. Stowe, J. Tower *et al.*, Neutron detection with $LiInSe_2$, in *Hard X-Ray, Gamma-Ray, and Neutron Detector Physics XVII* (SPIE, Bellingham, WA, 2015), Vol. 9593, pp. 20–32.
[49] E. Tupitsyn, P. Bhattacharya, and E. Rowe, Single crystal of $LiInSe_2$ semiconductor for neutron detector, Appl. Phys. Lett. **101**, 202101 (2012).
[50] E. E. Haller, N. P. Palaio, M. Rodder, W. L. Hansen, and E. Kreysa, NTD germanium: A novel material for low temperature bolometers, in *Neutron Transmutation Doping of Semiconductor Materials*, edited by R. D. Larrabee (Springer, New York, 1984), pp. 21–36.
[51] F. A. Danevich, V. Ya. Degoda, L. L. Dulger, L. Dumoulin, A. Giuliana, P. de Marcillac *et al.*, Growth and characterization of a $Li_2Mg_2(MoO_4)_3$ scintillating bolometer, Nucl. Instrum. Methods Phys. Res., Sect. A **889**, 89 (2018).
[52] V. Novati, L. Berge, L. Dumoulin, A. Guiliana, M. Mancuso, P. de Marcillac, S. Marnieros, E. Olivieri, D. V. Poda, M. Tenconi, and A. S. Zolotarova, Charge-to-heat transducers exploiting the Neganov-Trofimov-Luke effect for light detection in rare-event searches, Nucl. Instrum. Methods Phys. Res., Sect. A **940**, 320 (2019).
[53] C. Alduino, K. Alfonso, D. R. Artusa, F. T. Avignone III, O. Azzolini, T. I. Banks *et al.*, Analysis techniques for the evaluation of the neutrinoless double-β decay lifetime in ^{130}Te with the CUORE-0 detector, Phys. Rev. C **93**, 045503 (2016).
[54] O. Azzolini, M. T. Barrera, J. W. Beeman, F. Bellini, M. Beretta, M. Biassoni *et al.*, Analysis of cryogenic calorimeters with light and heat read-out for double beta decay searches, Eur. Phys. J. C **78**, 734 (2018).
[55] E. Andreotti, C. Arnaboldi, F. T. Avignone III, M. Balata, I. Bandac, M. Barucci *et al.*, ^{130}Te neutrinoless double-beta decay with CUORICINO, Astropart. Phys. **34**, 822 (2011).
[56] S. Di Domizio, F. Orio, and M. Vignati, Lowering the energy threshold of large-mass bolometric detectors, J. Instrum. **6**, P02007 (2011).
[57] E. Andreotti, C. Brofferio, L. Foggetta, A. Giuliani, B. Margesin, C. Nones, M. Pedretti, C. Rusconi, C. Salvioni, and M. Tenconi, Production, characterization, and selection of the heating elements for the response stabilization of the CUORE bolometers, Nucl. Instrum. Methods Phys. Res., Sect. A **664**, 161 (2012).
[58] D. Q. Adams, C. Alduino, K. Alfonso, F. T. Avignone III, O. Azzolini, G. Bari *et al.*, Measurement of the $2\nu\beta\beta$ Decay Half-Life of ^{130}Te with CUORE, Phys. Rev. Lett. **126**, 171801 (2021).
[59] O. Azzolini, J. W. Beeman, F. Bellini, M. Beretta, M. Biassoni, C. Brofferio *et al.*, Evidence of Single State Dominance in the Two-Neutrino Double-β Decay of ^{82}Se with CUPID-0, Phys. Rev. Lett. **123**, 262501 (2019).
[60] E. Armengaud, C. Augier, A. S. Barabash, F. Bellini, G. Benato, A. Benoit *et al.*, Precise measurement of $2\nu\beta\beta$ decay of ^{100}Mo with the CUPID-Mo detection technology, Eur. Phys. J. C **80**, 674 (2020).
[61] C. Alduino, K. Alfonso, D. R. Artusa, F. T. Avignone III, O. Azzolini, T. I. Banks *et al.*, Measurement of the two-neutrino double-beta decay half-life of ^{130}Te with the CUORE-0 experiment, Eur. Phys. J. C **77**, 13 (2017).
[62] A. Caldwell, D. Kollár, and K. Kröninger, BAT—The Bayesian analysis toolkit, Comput. Phys. Commun. **180**, 2197 (2009).
[63] Y. Iwata, N. Shimizu, T. Otsuka, Y. Utsuno, J. Menéndez, M. Honma, and T. Abe, Large-Scale Shell-Model Analysis of the Neutrinoless $\beta\beta$ Decay of ^{48}Ca, Phys. Rev. Lett. **116**, 112502 (2016).
[64] J. Menéndez, A. Poves, and E. Caurier, Disassembling the nuclear matrix elements of the neutrinoless $\beta\beta$ decay, Nucl. Phys. **A818**, 139 (2009).
[65] M. Horoi and A. Neacsu, Shell model predictions for ^{124}Sn double-β decay, Phys. Rev. C **93**, 024308 (2016).
[66] J. Barea, J. Kotila, and F. Iachello, $0\nu\beta\beta$ and $2\nu\beta\beta$ nuclear matrix elements in the interacting boson model with isospin restoration, Phys. Rev. C **91**, 034304 (2015).
[67] J. Toivanen and J. Suhonen, Microscopic quasiparticle-phonon description of odd-mass $^{127-133}$Xe isotopes and their β decay, Phys. Rev. C **57**, 1237 (1998).
[68] J. Allison, K. Amako, and J. Apostolakis, Recent developments in GEANT4, Nucl. Instrum. Methods Phys. Res., Sect. A **835**, 186 (2016).
[69] S. S. Wilks, The large-sample distribution of the likelihood ratio for testing composite hypotheses, Ann. Math. Stat. **9**, 60 (1938).
[70] D. E. Watt and R. N. Glover, A search for radioactivity among the naturally occurring isobaric pairs, Philos. Mag. **7**, 105 (1962).
[71] G. B. Beard and W. H. Kelly, Beta decay of naturally radioactive In^{115}, Phys. Rev. **122**, 1576 (1961).
[72] R. P. Feynman and M. Gell-Mann, Theory of the Fermi Interaction, Phys. Rev. **109**, 193 (1958).

[73] M. Haaranen, J. Kotila, and J. Suhonen, Spectrum-shape method and the next-to-leading-order terms of the β-decay shape factor, Phys. Rev. C **95**, 024327 (2017).

[74] J. Kostensalo, J. Suhonen, J. Volkmer, S. Zatschler, and K. Zuber, Confirmation of g_A quenching using the revised spectrum-shape method for the analysis of the ^{113}Cd β-decay as measured with the COBRA demonstrator, Phys. Lett. B **822**, 136652 (2021).

[75] A. Armatol, E. Armengaud, W. Armstrong, C. Augier, F. T. Avignone III, O. Azzolini *et al.*, Novel technique for the study of pileup events in cryogenic bolometers, Phys. Rev. C **104**, 015501 (2021).

[76] A. Kumar, P. C. Srivastava, J. Kostensalo, and J. Suhonen, Second-forbidden nonunique β^- decays of ^{24}Na and ^{36}Cl assessed by the nuclear shell model, Phys. Rev. C **101**, 064304 (2020).

[77] A. Kumar, P. C. Srivastava, and J. Suhonen, Second-forbidden nonunique β^- decays of ^{59,60}Fe: possible candidates for g_A sensitive electron spectral-shape measurements, Eur. Phys. J. A **57**, 225 (2021).

[78] H. Ejiri, J. Suhonen, and K. Zuber, Neutrino-nuclear responses for astro-neutrinos, single beta decays and double beta decays, Phys. Rep. **797**, 1 (2019).